A micro particle shadow velocimetry (mu PSV) technique to measure flows in microchannels

Journal Article

Author(s):
Khodaparast, Sepideh; Borhani, Navid; Tagliabue, Giulia; Thome, John Richard

A micro particle shadow velocimetry (µPSV) technique to measure flows in microchannels

Sepideh Khodaparast · Navid Borhani ·
Giulia Tagliabue · John Richard Thome

Abstract A micro particle shadow velocimetry (µPSV) system based on back-lit illumination and forward scatter observation of light from non-fluorescent particles has been developed. Relatively high luminous efficiencies and particle image contrasts were achieved by using the condenser stage of a standard transmitted light microscope and a continuous incoherent collimated light emitting diode (LED). This paper includes a critical review of the operating principles, benefits and practical problems associated with the predominant epifluorescent micro particle image velocimetry (µPIV) technique, and the less common light scattering µPIV methods of which µPSV is a development. This µPSV system was then successfully used to measure axial velocity profiles in a 280-µm-diameter circular channel up to a Reynolds number of 50 which corresponds to peak velocities of around 0.4 m/s. These velocity profiles were then integrated to provide instantaneous flow rates on the order of 100 µl/min to an accuracy of ±5 % relative to average flow rates determined using a digital balance. Due to the incoherent nature of the LED light source, the back-lit forward scatter observation mode and the applied refractive index matching system, the location of the test section walls and thus the local velocity fields were also accurately obtained. As a result of this, µPSV provides a low cost and safe way to investigate microfluidics, especially in lab-on-a-chip applications where the necessary optical access through transparent test sections is often available.

S. Khodaparast · N. Borhani (✉) · J. R. Thome
Laboratory of Heat and Mass Transfer (LTCM),
École Polytechnique Fédérale de Lausanne (EPFL),
Lausanne, Switzerland
e-mail: navid.borhani@epfl.ch

G. Tagliabue
Laboratory of Thermodynamics in Emerging Technologies
(LTNT), Eidgenössische Technische Hochschule Zürich
(ETHZ), Zurich, Switzerland

1 Introduction

The increasing demand for microfluidic systems, such as micro heat exchangers, microreactors and biomedical lab-on-a-chip devices, has made the fundamental understanding of fluid dynamics at such small length scales an inevitable challenge in many fields of science. Moreover, providing a deeper understanding of the physical phenomena involved, this information can be used to develop accurate prediction models and design guidelines for the production and commercialisation of more performant devices. This requires not only the measurement of time-averaged global quantities such as mass flow rates, pressure drops and temperatures, but also time-resolved details of local velocity fields at critical locations within the device. However, this is difficult to achieve due to the relatively high sensitivity of the sensors required to measure the small physical quantities encountered in microfluidics. In addition, the limited space available for installing instrumentation on microdevices, without causing significant perturbations to the flows under investigation, poses a significant practical problem. There is also a special need within the fields of biomedical and lab-on-a-chip microfluidics that diagnostic techniques can be safely and cheaply applied by researchers from a broad range of backgrounds and expertise levels.

As a result of the above requirements, there has been considerable research activity over the last decade to develop non-intrusive optical techniques with the high spatio-temporal resolutions required for microfluidic

applications. In particular, the application of particle image velocimetry (PIV) to microlength scales, in order to infer the fluid velocity fields from image sequences showing the motion of suspended tracer particles (Raffel et al. 2007), has been a very active field with the development of micro particle image velocimetry (μPIV) using epifluorescent microscopy by Santiago et al. (1998) being a key milestone. This now established and predominant technique requires the flow to be seeded with fluorescent particles whose physical properties are chosen so that they faithfully follow and respond to the local velocity fields. The region of interest (ROI) in the flow is then volumetrically illuminated by light at the characteristic excitation wavelength λ_X of the particles, thus causing them to fluoresce and emit light at a specific higher wavelength λ_M. On fluorescence, the particles act as point sources radiating light spherically. The combined light from the ROI is then low-pass filtered, thus allowing only the emission component to reach and be recorded by the camera imaging array, see Fig. 1a. This filtering enhances the contrast between the particle images and their background. The fundamental aspect of this technique is that the image of the particles on the plane of interest in the illuminated volume, across which the velocity field is desired, is isolated by using the very narrow depth of field of a high numerical aperture microscope lens, see Meinhart et al. (2000a). The resulting particle images comprise bright particles against a dark background whose contrast is produced purely by their fluorescence.

However, epifluorescent μPIV suffers from very low luminous efficiencies. Namely, with typical particle seeding densities and diameters, about 99.9 % of the incident illumination on the test section is transmitted through the volume without interacting with the particles or contributing to the particle image contrast; see Bohren and Hoffman (1983). Subsequently, since the quantum yield of the fluorescent particles is around 10 % (Ando and Kawaguchi 2005), only a fraction of the incident photons are remitted. Further significant losses also arise from a number of sources, these include (1) transmission and reflectivity losses at each component along the illumination and imaging optical trains of the microscope, particularly at the filters, beam splitters and dichroic mirrors; and (2) losses due to the spectral sensitivity of the camera imaging array. Therefore, the intensity of the images of static particles in the fluid recorded by the camera is on the order of 10^6 times smaller than the total illumination intensity of the light source (Nikon 2012). This contrast is further reduced due to the multiple scattering of the emitted light from neighbouring particles in the ROI, and possible fluorescence of materials used to fabricate the test section.

Most significantly for PIV applications, the intensity of the particle images, and thus the image contrast, decreases if the particles are in motion at the same illumination intensity. This is caused by the requirement to freeze the particle images in each recorded frame by decreasing the image exposure time or illumination pulse width, thus preventing them from streaking. As a result of this, in order
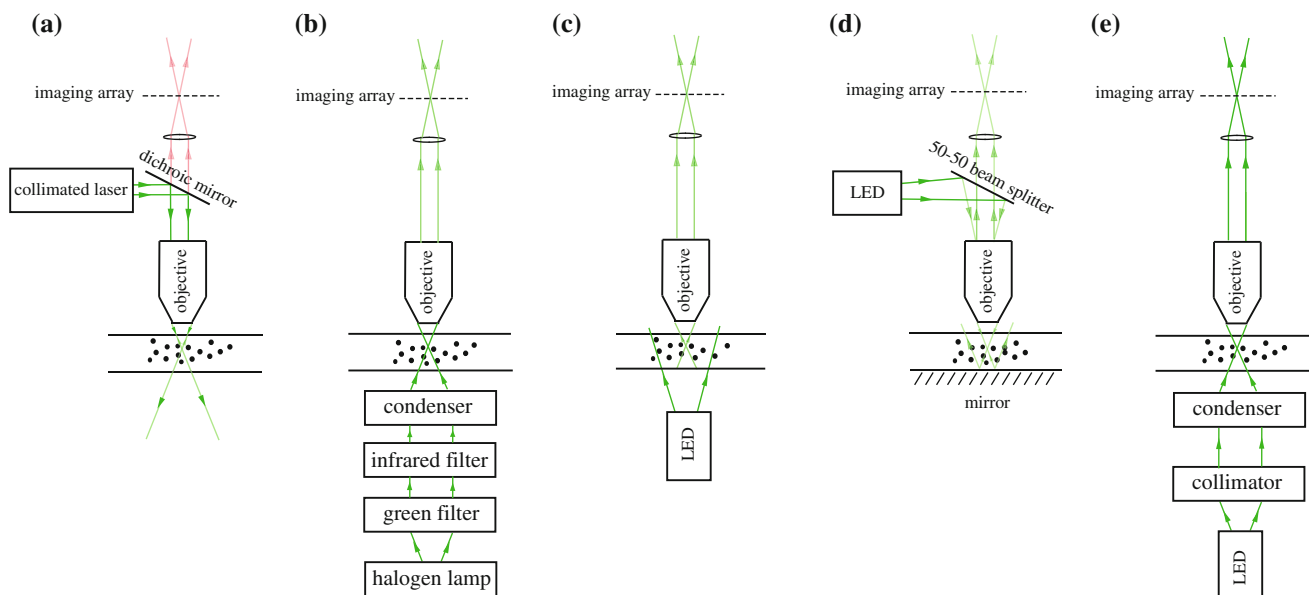
Fig. 1 Schematic of different optical arrangements used for micro particle image velocimetry: **a** laser front-lit epifluorescent μPIV, **b** halogen back-lit forward scatter with condenser (Koutsiaris et al. 1999), **c** LED back-lit forward scatter (Bitsch et al. 2005), **d** LED front-lit forward scatter with mirror (Hagsäter et al. 2008) and **e** the present LED back-lit forward scatter μPSV with condenser

to obtain particle images with sufficient contrast and thus signal-to-noise ratio (SNR) for PIV processing, the required illumination intensity increases with increasing flow velocities. Therefore, due to its poor light efficiency and the need to prevent streaking of the recorded particle images, the use of coherent high-powered pulsed lasers and high sensitivity cameras, often with image intensifiers or cooled imaging arrays, has become commonplace for epi-fluorescent μPIV applications. Furthermore, in order to study faster microflows, there has been a trend towards the use of more powerful lasers with shorter pulse widths and separations, as highlighted by review articles such as Lindken et al. (2009), Williams et al. (2010) and Wereley and Meinhart (2010), which can lead to physical 'shot' damage of the test section or optics.

Since the coherent high-power laser light source is typically not only the most expensive component of an epifluorescent μPIV system but also poses a number of important health and safety issues, there is a clear motivation to use less powerful, longer life, and thus cheaper solutions such as super bright incoherent light emitting diodes (LEDs) with finite continuous spectral bandwidths. Therefore, due to the lower light intensities provided by LEDs, the optimal use of the available light is paramount for the design of any efficient and economical micro particle imaging system, be they epifluorescent or scattered light in nature. Ideally, this should be achieved by maximising the particle image contrast to span the entire dynamic range of the camera whilst using the minimum incident illumination intensity. Practically, this involves optimising four criteria as discussed below.

Firstly, the microimaging system should be designed to minimise light losses along both its illumination and imaging optical trains, for example, by matching the numerical apertures of its components, avoiding the use of fibre optics and minimising transmission lengths. Practically, this optimisation should be achieved by using a minimally modified standard microscope system to reduce costs. As a result of this optimisation, not only can cheaper light sources such as LED be used but problems with dissipating the heat and vibrations generated by larger devices can be avoided. On a related note, the wavelength of the illumination source should also match the maximum spectral sensitivity of the camera imaging array. This is easier to achieve by replacing cheap LEDs rather than purchasing tunable coherent lasers.

Secondly, the contrast between the particle images and their background, for a given illumination intensity, should be maximised. This optimisation has a number of benefits, including (1) using the complete dynamic range of the camera imaging array, and thus increasing the SNR and accuracy of the subsequent velocity interrogations by techniques such as digital particle image velocimetry

(DPIV) (Willert and Gharib 1991); (2) allowing the use of shorter exposure times or illumination pulses, thus permitting faster flow velocities to be measured; and (3) requiring less sensitive and thus cheaper cameras, and eliminating the need for expensive image intensifiers.

Thirdly, the illumination intensity incident on the test section should be the minimum necessary to obtain satisfactory particle image contrasts for PIV post-processing. This optimisation minimises thermal effects which can cause severe problems in the testing of microfluidic devices; these include (1) the magnitude of parasitic flows induced by particle motions driven by photophoresis and buoyancy forces; (2) the possibility of localised heating causing thermo-convective instabilities, bubble nucleation or dryout; (3) damage to the test section, especially when pressurised, due to differential thermal expansion of its components and fatigue due to cyclic heating; (4) damage to sensitive samples especially in biomedical applications; and (5) local changes in the physical properties of the working fluid. Minimising the incident illumination intensity also reduces the photo bleaching of biological samples in the test section.

Finally, when liquid flows are observed through transparent structures, a difference between the refractive indices of the working fluid and the test section materials can lead to optical distortion of the ROI due to refraction of the light. As well as leading to the wrong spatial assignment of erroneous velocity vectors, this also increases light losses at such interfaces. Furthermore, total internal reflection of light at curved interfaces masks their true location. These undesirable effects can be minimised by suitable refractive index matching strategies (Budwig 1994), and should be applied to all particle imaging systems when possible, including epifluorescent μPIV.

In order to obtain optimal particle images for velocimetry using non-fluorescent particles, one must consider how light interacts with the tracer particles: when a beam of monochromatic light is incident on a single spherical particle, whose diameter is on the order of the wavelength of light and is suspended in an infinite transparent medium, it becomes scattered. This scattering is due to a number of different mechanisms including reflection, refraction, interference, diffraction and absorption of the light by the particle. Furthermore, it depends on several factors including the ratio of the refractive indices of the particle n_p to the surrounding medium n_o, the particle diameter ϕ_p, and the intensity I_0 and wavelength λ of the incident light. The exact nature of this scattering is predicted by the Mie solution of Maxwell's equations; see Bohren and Hoffman (1983), Ovryn and Izen (2000) and Ovryn (2000) for details. However, for the case relevant to the present study, namely the scattering of monochromatic light with a wavelength $\lambda = 530$ nm from a non-absorbing $\phi_p = 1$ μm

diameter spherical particle of refractive index $n_p = 1.59$ surrounded by a medium with refractive index $n_o = 1.33$, the angular intensity dependence $S(\alpha)$ of the Mie scattering is approximately shown in Fig. 2. As can be seen from this polar plot, which has a logarithmic radial intensity scale, light is scattered into lobes which are axisymmetric about the illumination direction. Therefore, the total scattered light $\bar{S}_\theta$ collected by the acceptance cone of a microscope objective, focused on the particle centre, strongly depends on the observation angle θ relative to the illumination direction; where the half angle θ_L of this cone is given by the numerical aperture $NA = n_{air} \sin \theta_L$ of the microscope objective. By numerically integrating the Mie scattering lobes over an acceptance cone, the collected light intensity for different observation angles $\bar{S}_\theta$ and lens numerical apertures can be estimated, thus allowing the corresponding particle image contrast $C_\theta = |\bar{S}_\theta - B_\theta|$ to be determined; where B_θ is the background intensity for an observation angle of θ relative to the illumination direction. In the present case, with $\theta_L \approx 36°$, this calculation indicates that the particle image contrast obtained with the front scatter $\theta = 0°$ mode is around 50 times greater than that from the back scatter $\theta = 180°$ mode at the same incident illumination intensity; where the back ground intensities were assumed to be $B_{0°} = I_0$ and $B_{180°} = 0$, respectively. Similarly, the contrast provided by the side scatter $\theta = 90°$ mode, which is the dominant mode in macroscale PIV using laser light sheet illumination, is around 10 times greater than that from the back scatter $\theta = 180°$ mode, assuming the background intensity $B_{90°} = 0$. Therefore, the front scatter mode provides dark particle 'shadows' on a bright background, whilst the back and side scatter modes provide bright particles on a dark background. Using similar arguments for a fluorescing particle with a quantum yield of 10 % which emits its energy spherically upon excitation by a monochromatic light beam of suitable wavelength, it can be shown that the
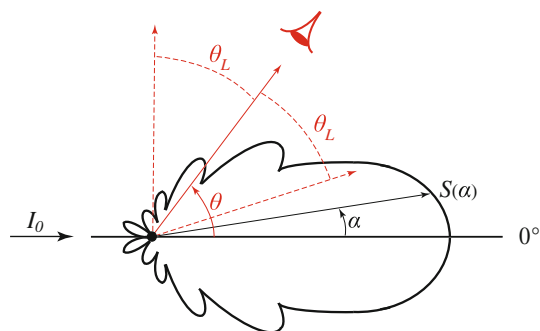
particle image contrast obtained by recording its emission component is about 10 % that achieved with the front scatter observation of a non-fluorescing particle at the same illumination intensity. In reality, the collected light and thus particle image contrasts for all observation modes are affected by massive multiple scattering of light from neighbouring particles in the suspension, reflections from surfaces, finite apertures and observation distances, off axis observation of the particles, absorption of light by the particles, and the finite spectral bandwidth of the light source.

Observing that the front scatter mode provides greater particle image contrast than the side scatter mode for the same illumination intensity using non-fluorescent particles, a relatively small number of previous researchers developed macro-PIV systems using standard camera lenses to observe ROI greater than a few millimetres in size; where back-lit volumetric illumination was provided by relatively cheaper super bright LEDs operating in continuous or pulsed modes. Such systems include the particle shadow velocimetry (PSV) system developed by Estevadeordal and Goss (2005, 2006), the miniature particle image velocimetry (MPIV) system of Chételat and Kim (2002), the two-phase system of Bröder and Sommerfeld (2007) and the high-powered pulsed technique of Willert et al. (2010).

Similarly, since the forward scatter mode using non-fluorescent particles provides greater particle image contrast than obtained from fluorescing particles for the same incident illumination intensity, a few researchers have explored the application of the front scatter mode to microfluidic applications by using high numerical aperture microscope objectives. Such systems, sometimes referred to as bright field or transmission mode μPIV, include those developed by Koutsiaris et al. (1999), Bitsch et al. (2005) and Hagsäter et al. (2008). The system developed by Koutsiaris et al. (1999) is shown in Fig. 1b. In this system, based on a transmitted light microscope, a 20-W halogen lamp was used to provide back illumination to a transparent refractive index matched test section using a condenser lens. Due to the broad spectrum nature of this 'hot' light source, two filters were used along its illumination optical train: one to remove its infra-red component thus reducing undesirable heating effects on the observed flow, and a second green filter to reduce chromatic aberrations thus enhancing particle shadow contrasts. Therefore, although the condenser lens efficiently focused the remaining light onto the ROI, a large proportion of the light provided by the halogen light source was lost due to the filters, thus limiting the system to the study of low-speed flows up to 4 mm/s. Another limitation of this set-up is that the halogen lamp cannot be pulsed for higher-speed flow applications. The optical system used by Bitsch et al. (2005), as shown in Fig. 1c, comprised a single non-collimated diverging continuous 1-W LED placed under a

Fig. 2 Polar intensity dependence $S(\alpha)$ of the Mie scattering of light I_0 by a spherical particle, where θ is the observation angle relative to the illumination direction, and θ_L is the half angle of the acceptance cone of the microscope objective lens

transparent test section to provide back illumination through a frosted diffuser screen. As a result of this configuration, the system suffers from low incident illumination intensities, large light losses and alignment problems. This was later improved upon by Hagsäter et al. (2008), who used the 50–50 beam splitter of a standard reflected light microscope to provide in-line top illumination of the test section through a microscope objective, see Fig. 1d. Illumination was provided by a pulsed high-power LED driven by a 26.4-W power supply. In their most optimal configuration, the transmitted light was then reflected back through the transparent test section from a mirror before being collected by the microscope objective. Although this novel optical set-up overcame problems related to the low power densities of LED by using the objective to focus their light onto the ROI, the use of the beam splitter caused a 50 % loss of the illumination light source intensity and a 50 % decrease in the collected particle image contrast. Further luminous inefficiencies also arose due to the divergence of the illumination light cone on reflection from the mirror and the reduction in the particle image contrast due to the mixed back-front scattering observation mode.

Regarding the simultaneous location of surfaces whilst using particle imaging techniques, one advantage of epi-fluorescent μPIV is that by cutting off the excitation wavelength with a low-pass filter, problems with specular reflections, glare and interference pattern artifacts obtained when coherent laser light is incident on surfaces or interfaces are greatly reduced. As a result of this, flows near surfaces can be reliably resolved. However, problems may still arise due to reflections of the scattered fluorescing light component especially for high seeding concentrations and high illumination intensities. Furthermore, if a particular application requires the motions and/or shapes of submerged structures such as swimming microorganisms to be resolved simultaneously with the flowfield, then such structures must also fluoresce accordingly. This 'doping' may not only be toxic to the biomaterial but also interfere with any occurring chemical reactions. On the other hand, the use of scattered incoherent LED light for particle imaging not only eliminates problems arising when coherent light is incident on surfaces or interfaces, but it also allows the motion and shape of submerged structures in the observed flowfield to be easily determined without doping. In fact, such back-lit 'shadowgraphy' techniques have been previously used to accurately determine the location of solid surfaces and phase boundaries in PIV studies; for example, see Lindken and Merzkirch (2002), Nogueira et al. (2003) and Bröder and Sommerfeld (2007).

Therefore, noting the above observations, a new micro particle shadow velocimetry μPSV system was developed in the present study by combining the most efficient elements of each previous set-up. Namely, this system is based on the in-line back illumination and forward scatter observation of light from non-fluorescent tracer particles in the ROI, thus providing the greatest particle image contrast for a given incident illumination intensity and particle choice. Relatively high luminous efficiencies were achieved by using a continuous incoherent collimated LED light source placed under the condenser stage of a standard transmitted light microscope; see Fig. 1e. Not only did this condenser focus the LED light uniformly onto the ROI, but it also matched the illumination cone angle with the numerical aperture of the microscope objective, thus minimising light losses and enhancing the particle image contrasts. Furthermore, refractive index matching was implemented in order to minimise optical distortions of the recorded ROI, to eliminate total internal reflection at the curved channel walls thus allowing their accurate location, and to minimise light losses due to reflectivity and scatter at the interfaces.

The following sections provide a description of the practical implementation of this μPSV system, including factors governing the quality of the particle shadow images. The developed system was then successfully used to measure axial velocity profiles in a 280-μm-diameter circular channel up to a Reynolds number of 50 which corresponds to peak velocities of 0.4 m/s. These velocity profiles were then integrated to provide instantaneous flow rates on the order of 100 μl/min to an accuracy of ±5 % relative to average flow rates determined using a digital balance.

2 Experimental facility and measurement technique

A transparent test section was used to allow back-lit LED illumination of the ROI, namely the centre plane of a circular microchannel. This test section, shown in Fig. 3a, b, comprised a straight horizontal fluorinated ethylene propylene (FEP) circular tube with a measured internal diameter d_i of 280 μm and an outer diameter d_o of 1,600 μm. The FEP tube test section was 10 cm long, thus ensuring that the flow at its observed midspan was fully developed and independent of entrance and exit effects.

This FEP tube was submerged inside a water bath held within a transparent plexiglass container. If necessary, the temperature of the water pool can also be regulated in biomedical microfluidic studies to protect the samples. Demineralised water was then pumped through the test section by a Mitos P-pump which provided a steady non-oscillating flow, as shown schematically in Fig. 3c. Since the refractive indices of the working fluid, tube material and surrounding water pool were all approximately 1.33, and the test section was observed through the horizontal flat surface of the water pool, optical distortions of the ROI

Fig. 3 Experimental set-up:
a schematic and **b** photograph
of the refractive index matched
FEP tube test section and water
pool, **c** schematic of the facility
and **d** photograph of the
microscope assembly
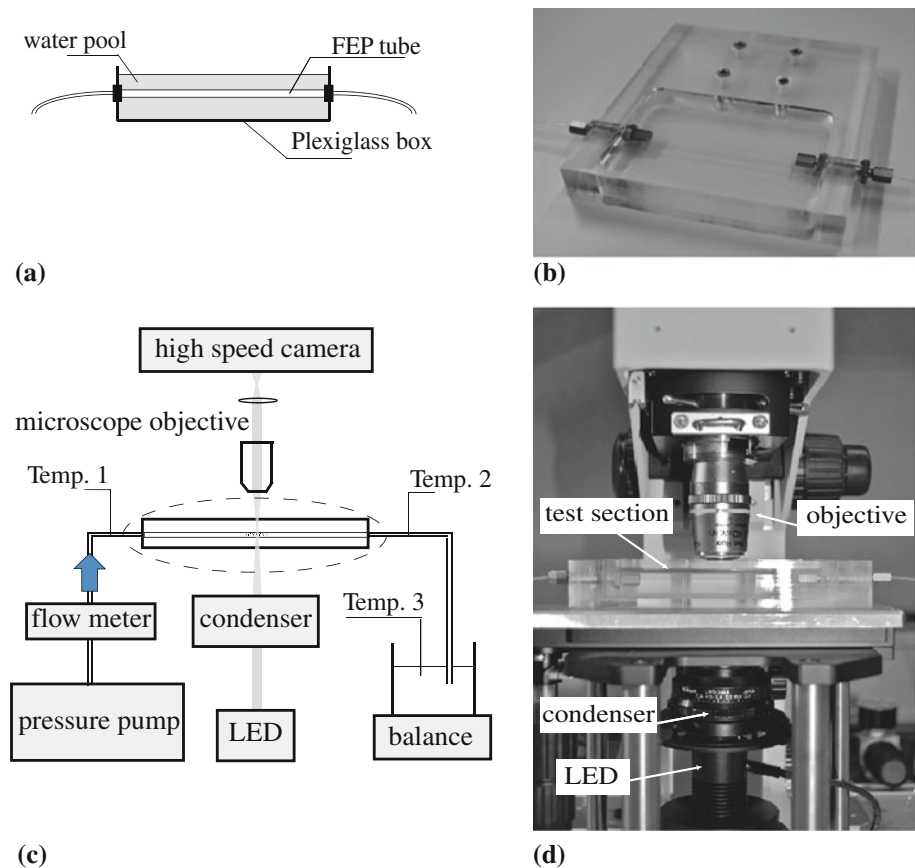
due to refraction at the outer and inner curved surfaces of the tube were minimised (Budwig 1994). As a result of this, no numerical warping of the obtained images was necessary to compensate for optical distortions. Furthermore, since the refractive index matching also prevented total internal reflection, the flowfield close to the channel walls could also be resolved.

The reference average volumetric flow rate through the test section during each experimental run was determined to 1 % accuracy by using a digital balance to measure the total mass flow at the exit of the system over a time period of 3 minutes, where the temperature of the collected water was used to determine its density. Two different Mitos flow rate sensors were also used to provide a real-time indication of the flow rate when setting the driving pressure of the pump prior to each experimental run; these had flow rate ranges of 1–5 μl/min and 0.2–5 ml/min, respectively, and were calibrated in situ using the digital balance. They had an advertised accuracy of 5 % of their maximum flow rates. The average of the working fluid temperatures measured before and after the water pool was used to determine its physical properties at the ROI. This temperature ranged from 24 to 27 °C depending on operating conditions.

In order to carry out micro particle shadow velocimetry (μPSV), the transparent test section was mounted above the

Nikon LWD 0.65 condenser of a Nikon Eclipse E600-FN transmitted light microscope. Continuous in-line volumetric back illumination of the ROI was then provided by mounting a green Thorlabs M530L2 LED unit below the microscope condenser, see Fig. 3c, d. This LED, driven by a Thorlabs LEDD1B 10 V 1,200 mA power supply, provided a maximum beam power of 475 mW at a nominal wavelength of 530 nm. In order to reduce radiant heating of the test section and the tracer particles, the LED was only illuminated when μPSV measurements were being taken, and care was taken to only use the minimum LED power necessary to obtain satisfactory μPSV images at each flow rate. Furthermore, since the test section was not in contact with the LED, it was unaffected by heat dissipated by its electronics.

The particle shadow images were recorded using a high-speed Photron FASTCAM SA3 greyscale camera. This camera possessed a 1,024 × 1,024 pixel detector array, with each pixel being 17 μm × 17 μm in size. Image sampling rates up to 10 kHz and exposures up to 5 μs were used in this study. The efficiency and uniformity of the illumination system were increased by using the microscope condenser to focus the light onto the ROI, and to match the divergence angle of the illumination cone with the numerical aperture of the microscope objective.

Furthermore, a frosted polymeric diffuser was placed directly above the LED element to further enhance illumination uniformity.

2.1 Factors affecting the particle shadow intensity profiles and visibility

In order to determine the velocity profile across the entire 280 μm channel width, the illuminated ROI was observed through a long working distance Nikon Plan Fluor $40\times$ infinity corrected dry objective with a numerical aperture of $NA = 0.6$ and thus $\theta_L \approx 36°$. The advertised optical depth-of-field (DOF) of this objective was approximately 2.5 μm (Nikon 2012), whilst that determined according to Inoué and Spring (1997) was approximately 3 μm. As well as recording the entire channel width on each video frame, by using a known calibration target, this objective was found to provide a field-of-view (FOV) of 665 μm $\times$ 665 μm on the camera array, and thus a spatial resolution of 0.65 μm/pixel.

To provide tracer particles for the velocimetry, the working fluid was seeded with polystyrene microspheres manufactured by Polysciences Inc. These colourless particles had a density of 1 g/cm^3 and a refractive index of 1.59. The quality of the recorded particle shadows depends sensitively on the system magnification, camera imagining array pixel size and particle diameter. Therefore, since the optical set-up and camera were fixed for this particular application, two tests were carried out to determine the optimal particle diameter:
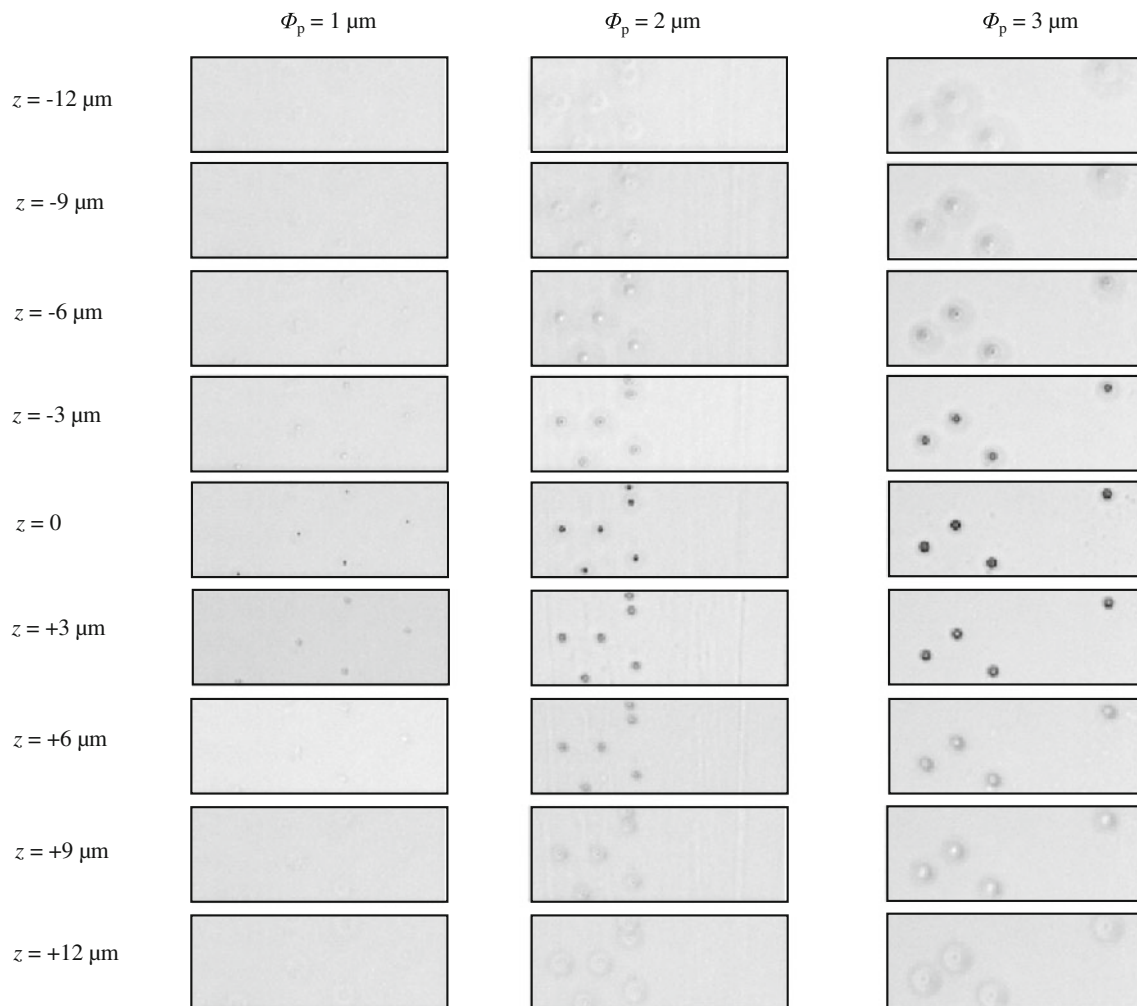
Firstly, particle shadow intensity profiles for 1-, 2- and 3-μm-diameter particles were obtained by recording the images of particles resting on a microscope slide submerged in water, see Fig. 4. Care was taken to ensure that the particles did not agglomerate in these images and that the illumination power was constant. The microscope was focused on the particles, such that the normal distance z between their location and the focal plane of the microscope objective was zero. As can be seen from Fig. 4, although the particle shadow contrasts remain almost constant, their image diameter increases as the particle diameter increases. Furthermore, for 1- and 2-μm-diameter particles, the intensity profiles display a single minimum, whilst ring-like profiles with two minima were observed for 3-μm-diameter particles.

Secondly, in order to estimate the contribution of particles not on the focal plane of the microscope objective inside an illuminated volume, the effect of defocusing on the recorded particle shadows was studied by varying z. The obtained images, shown in Fig. 5, indicate that defocusing produces ring-like artifacts which grow in size and amplitude as the particle diameters increase. Similarly, the visibility and thus background noise amplitude generated by particles not on the object plane (Olsen and Adrian 2000) was determined by measuring the peak particle shadow contrasts as a function of defocusing distance z for
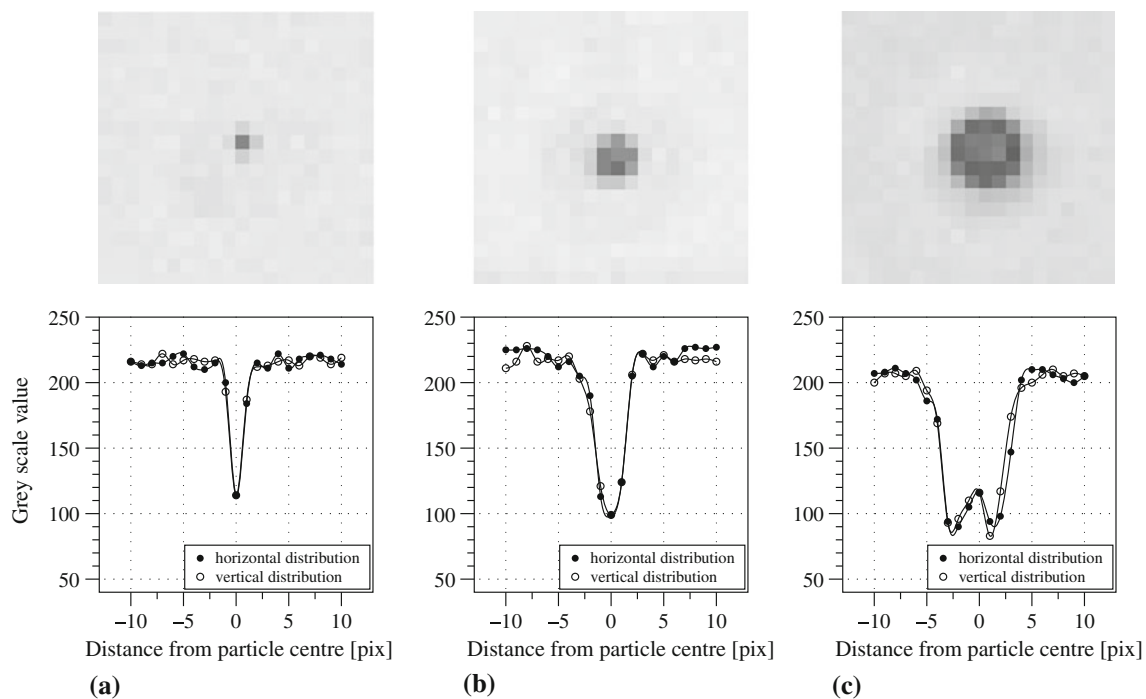
Fig. 4 Particle shadow intensity profiles for **a** 1-, **b** 2- and **c** 3-μm polystyrene particles resting on a microscope slide submerged in water at the same illumination power taken with the $40\times$ objective. The microscope is focused on the particles at $z = 0$

$\Phi_p = 1\ \mu m$ $\Phi_p = 2\ \mu m$ $\Phi_p = 3\ \mu m$

$z = -12\ \mu m$

$z = -9\ \mu m$

$z = -6\ \mu m$

$z = -3\ \mu m$

$z = 0$

$z = +3\ \mu m$

$z = +6\ \mu m$

$z = +9\ \mu m$

$z = +12\ \mu m$

Fig. 5 Particle shadow intensity profiles for 1-, 2- and 3-μm polystyrene particles, resting on a microscope slide submerged in water, as a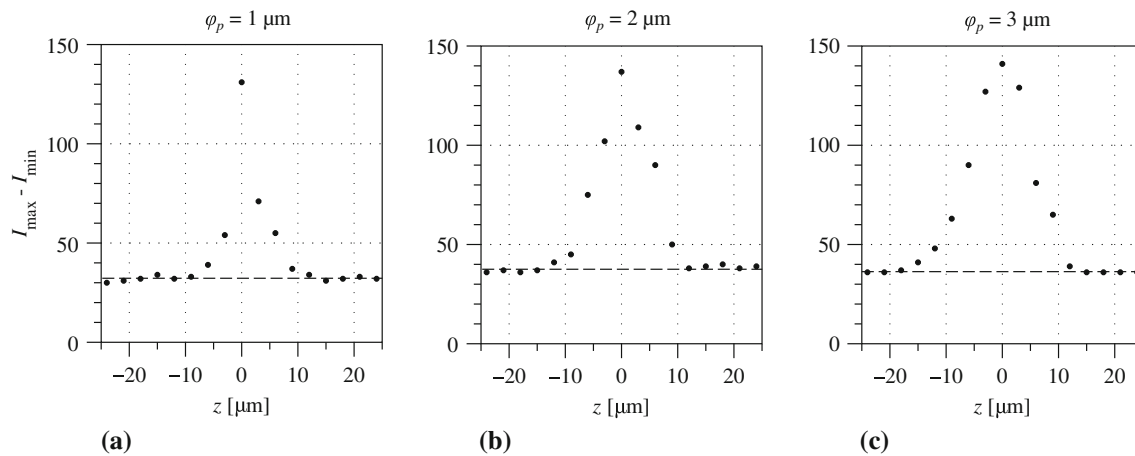 function of the distance z between the focal plane of the objective and the particle centres. The images were taken at the same illumination power with the 40× objective

1-, 2- and 3-μm-diameter particles. The results are shown in Fig. 6, where the dashed lines indicate the mean background image contrast in the absence of particles. As can be seen, relative to this conservative threshold contrast level, the visibility depth increases from 15 to 27 μm as the particle diameter increases from 1 to 3 μm.

The subsequent effect of these visibility depths on the accuracy of the evaluated velocity fields depends on the velocimetry technique used. However, decreasing the visibility depth typically increases the SNR of the recorded image sequences. This then leads to better velocity results especially in regions of high shear normal to the object plane. For example, for epifluorescent μPIV using cross-correlation velocity interrogation, the depth-of-correlation increases from around 7.5 to 21 μm as the particle diameter increases from 1 to 3 μm for the same microscope objective used in the present

study (Olsen and Adrian 2000). These values are comparable to the visibility depths measured for the present μPSV system.

In addition to decreasing the response time of tracer particles to fluctuations in the velocity field, the above results indicate that the particle diameter should be minimised to obtain suitably shallow visibility depths, and prevent the formation of rings for in focus particles. However, in order to increase the sub-pixel accuracy of locating the particles for particle tracking velocimetry (PTV) or the cross-correlation peaks in DPIV, particle shadow diameters of approximately 3 pixels are desired (Raffel et al. 2007). Considering this, 1-μm-diameter particles were chosen for the present optical set-up and application, with the resulting 15-μm visibility depth effectively isolating the centre plane of the 280 μm channel with no image post-processing applied.

Fig. 6 Particle shadow contrasts for **a** 1-, **b** 2- and **c** 3-μm polystyrene particles, resting on a microscope slide submerged in water, as a function of the distance z between the focal plane of the objective and the particle centres. The images were taken at the same illumination power with the 40× objective. The *dashed lines* indicate the mean background image contrast in the absence of particles

2.2 Velocimetry

The free PIV software package JPIV (JPIV 2012) was used to process the obtained μPSV images. Since the laminar fully developed axisymmetric Poiseuille flow expected in the present study has velocity gradients only in the radial direction, rectangular interrogation windows of size 32×64 pixels were used for the cross-correlation velocity interrogations. By aligning the longer side of these windows with the flow direction, smearing of the axial velocity profile was reduced and the flow close to the channel walls was better resolved.

The recorded particle shadow images were interrogated via the cross-correlation technique to infer the fluid velocity field. In order to increase the SNR of the cross-correlations, the particle shadow images were thresholded beforehand to remove background features caused by illumination gradients and out-of-focus particles, see Santiago et al. (1998). The mean image of the recorded sequence was used to determine the threshold value for each case. As a result of this, out-of-focus particles had a reduced impact on the SNR of the cross-correlation function, especially in regions of high velocity gradients normal to the ROI. Fig. 7 shows a typical raw μPSV image, as well as its background and background removed results.

The magnitude of peak locking effects (Cholemari 2007), obtained by applying the above velocity interrogation technique to the recorded particle shadow sequences, was also investigated by determining the probability density function (PDF) of the fractional part of the particle displacements in pixels for a flow at $Re = 17.7$. The flowfield was obtained by cross-correlating only two frames. The almost uniform distribution shown in Fig. 8

indicates the absence of peak locking effects, thus indicating the high quality of the obtained images.

Although the particle seeding density was chosen to provide at least 10 particle images per IW, as shown in Fig. 7, due to the volumetric illumination used in microparticle imaging techniques, not all of these particles are in focus and thus able to contribute significantly to enhancing the signal-to-noise ratio of the cross-correlation function. It should be noted that the probability of finding a particle on the focal plane of the objective can be increased by increasing the particle seeding density. However, this would also result in an increase in the background noise level caused by out-of-focus particles, and an increase in the attenuation of the illuminating light as it passes through the test section. Therefore, since the flowfields of interest in the present study were found to be laminar and steady, the accuracy of the interrogated velocity vectors was increased by applying the cross-correlation averaging technique proposed by Meinhart et al. (2000b).

In order to identify the optimal number of cross-correlation functions to average, the volumetric flow rate was determined as a function of the number of image pairs used to calculate the average cross-correlation function. For each case, this was determined by integrating the velocity over the cross-sectional area of the tube whilst assuming the flow to be axisymmetric. It should be noted that the individual cross-correlation functions were not normalised before summation, thus minimising possible detrimental effects (Cierpka and Kähler 2012). Furthermore, due to the high frame rates used in this study, the averaged cross-correlations were not truly independent since some particles remained within a given interrogation window between successive
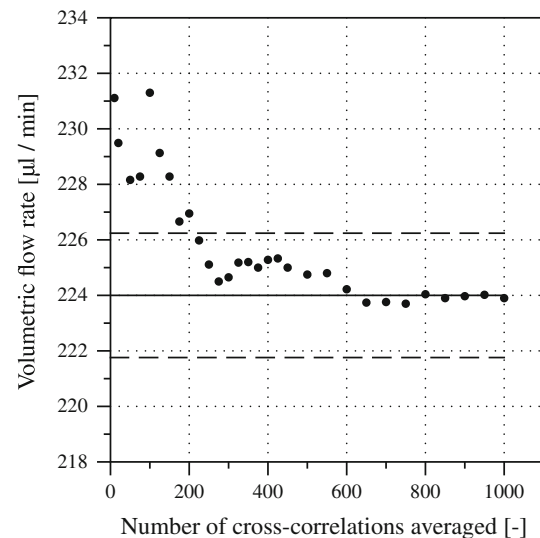
(a)   **(b)**   **(c)**
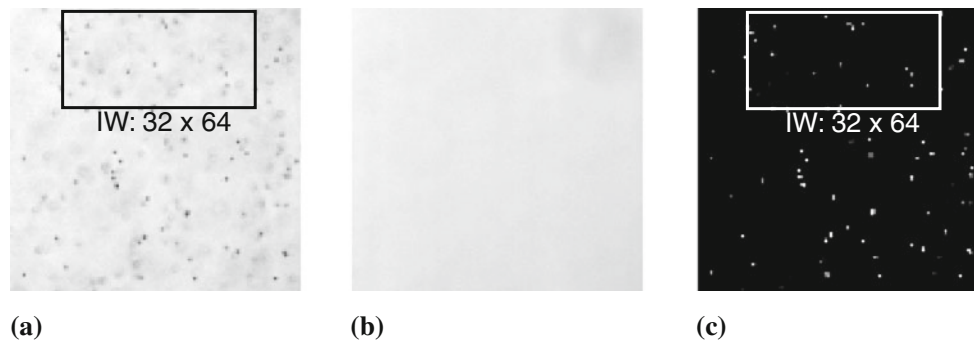
Fig. 7 a A typical 75 μm × 75 μm FOV μPSV image of 1-μm polystyrene particles suspended in water taken with the 40× objective, with its b mean background, and c background subtracted

results. A 32 × 64 pixels interrogation window has been superimposed on the images for reference
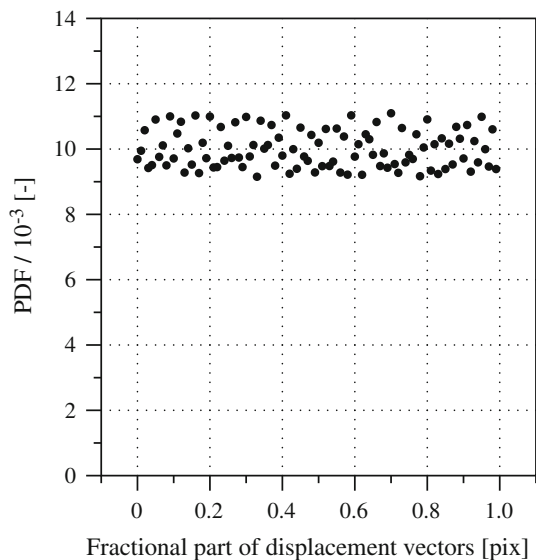
Fig. 8 Probability density function of the fractional part of the particle displacements in pixels at $Re = 17.7$ evaluated by applying the cross-correlation scheme to two sequential frames. The almost uniform distribution indicates the absence of peak locking effects

Fig. 9 The volumetric flow rate calculated by integrating the velocity profile over the cross-sectional area, at $Re = 17.7$ in a 280-μm-diameter tube, as a function of the number of cross-correlations averaged. The *dashed lines* indicate the ± 1 % error boundaries relative to the asymptotic value depicted by the *solid line*

samples; this number decreases with increasing flow velocities for a given frame rate. As expected, Fig. 9 indicates that the calculated volumetric flow rate approaches an asymptotic value as the number of cross-correlations averaged increases. This convergence, albeit from a flow rate only 3 % different from the asymptotic value determined from averaging 1,000 cross-correlations, is due to the increase in the signal-to-noise ratio of the interrogated cross-correlation functions because of the averaging. Therefore, as a comprise between the total sampling time and the obtained accuracy, 200 cross-correlations were averaged for all of the presented results since this value provides flow rates within 1 % of the asymptotic value. This value corresponds to a sampling time of 0.05 s at the imposed frame rate of 4,000 Hz, and thus effectively provides an instantaneous flow rate.

3 Results and discussion

3.1 Comparison between the performance of μPSV and epifluorescent μPIV systems

The performance of the developed μPSV system, with and without its condenser stage, was compared directly with that provided by a back-lit epifluorescent μPIV system using the same continuous 530-nm LED light source, 40× objective, camera and exposure time for particle diameters of 1 μm; see Fig. 10 for details. Fluorescent 1-μm-diameter polymer microspheres from Duke Scientific with $\lambda_X = 540$ nm and $\lambda_M = 620$ nm, and a 600- to 650-nm band-pass emission filter were used for the epifluorescent μPIV case. The particle images and intensity histograms of particles resting on a microscope slide
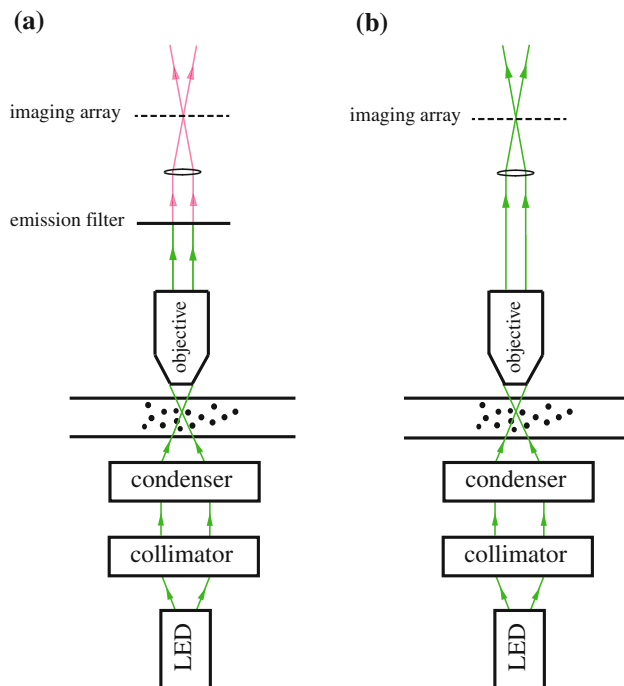
Fig. 10 Schematics showing the tested **a** LED back-lit epifluorescent μPIV and **b** μPSV systems

submerged in water are shown in Fig. 11. As can be seen from Fig. 11a, epifluorescent μPIV was unable to produce particle images even at the maximum power of the LED. This compares with the μPSV system which was able to produce particle shadows with high levels of contrast at 100 % of the available illumination intensity even without its condenser stage; see Fig. 11b. Furthermore, by including the condenser and thus decreasing light losses, the same particle shadow contrasts could be achieved with only 10 % of the available illumination intensity; see Fig. 11c. These result not only highlight the relatively high luminous efficiencies and contrasts obtained with the new μPSV system, but also the crucial role the condenser plays in the performance of the μPSV system.

These tests also indicated that the μPSV system was comparatively easy to optimise in practice: for a given flow application, one needs to determine the camera exposure time or illumination pulse width required to freeze the particle images. Then, the intensity of the illumination is increased until the background illumination level recorded by the camera with these settings is approximately 90 % of its dynamic range, thus preventing saturation of the recorded particle images.
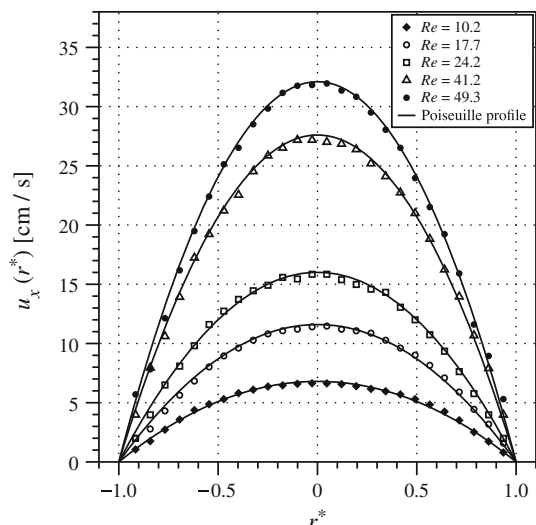
3.2 Velocity profiles

The developed μPSV system was then used to measure the velocity field across the centre plane of the 280-μm-diameter circular microchannel. The obtained axial
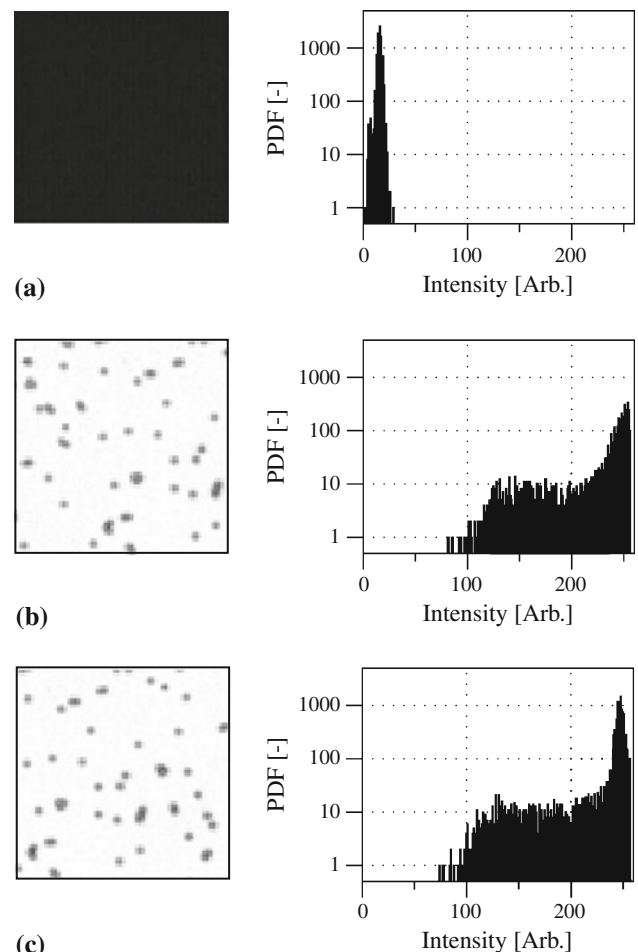
Fig. 11 Sample particle images and intensity histograms of 1-μm-diameter tracer particles, resting on a microscope slide submerged in water, obtained from the **a** LED back-lit epifluorescent μPIV set-up using 100 % of the available illumination power, the **b** μPSV system without its condenser using 100 % of the available illumination power, and the **b** μPSV system with its condenser using <10 % of the available illumination power. The same LED light source, 40× objective, camera and exposure time were used for all of the cases

velocity profiles $u_x(r^*)$ are shown in Fig. 12 for different Reynolds numbers $Re = \bar{u}d_i/v$ where $r^* = 2r/d_i$, r is the radial location, $\bar{u}$ is the mean flow velocity across the tube cross-sectional area as determined from the reference average flow rate provided by the digital balance, and v is the bulk kinematic viscosity. The good agreement with the expected theoretical parabolic Poiseuille velocity profiles, defined using $\bar{u}$, indicates the high accuracy provided by μPSV over a large range of flow velocities. In fact, the present system was able to accurately resolve velocities of up to 0.4 m/s across the ROI. The general underestimation of the velocity magnitude near the channel centreline, relative to the Poiseuille solution, can be attributed to the finite DOC and visibility depths associated with the use of volumetric illumination for micro particle imaging. As a result of this, out-of-focus particles have been found to

Fig. 12 Axial velocity profiles across the centre plane of a 280-μm circular tube as a function of Reynolds number *Re*

Fig. 13 Comparison of volumetric flow rates calculated using μPSV results with those obtained from digital balance measurements in a 280-μm tube. The *dashed lines* indicate the ±5 % error boundaries
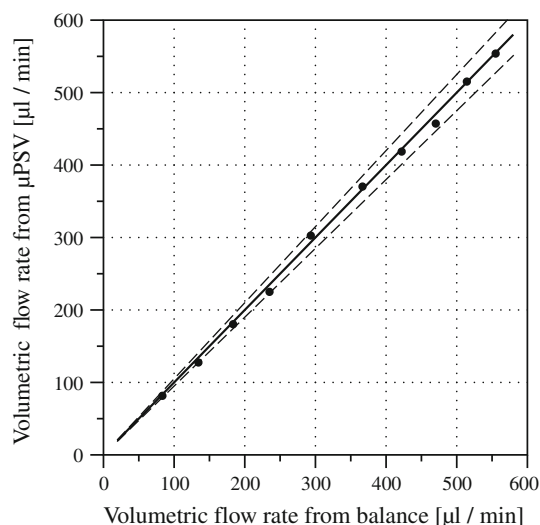
cause an underestimation of the true particle displacements on the focal plane, especially in regions where high velocity gradients exist normal to the focal plane, see Kloosterman et al. (2011).

The results also indicate that the absence of specular reflections, due to the incoherent nature of the LED light, also allowed velocities close to the wall to be accurately resolved. Furthermore, comparison between the measured and theoretical velocity profiles indicates that the applied refractive index matching strategy successfully minimised optical distortions of the ROI.

By assuming the flow to be axisymmetric, the experimental axial velocity profiles were integrated across the cross section of the tube to calculate the instantaneous volumetric flow rates. Figure 13 shows the comparison between these values and those determined from time-averaged measurements using the digital balance. As can be observed, the difference between the two is always <5 % across the range of flow rates studied. This difference is probably due to uncertainties in accurately measuring the tube diameter, or the longer time averages used in determining the flow rates from the balance. The high accuracy and sensitivity obtained by using μPSV suggests it can be used to non-intrusively measure even very low instantaneous flow rates in the multiple feed lines of microfluidic devices, thus reducing costs and problems with the limited space available for installing instrumentation.

4 Conclusions

A μPSV system has been developed with the aim of maximising the particle image contrast to span the entire dynamic range of the imaging array whilst using the minimum incident illumination intensity on the test section. This was achieved by combining and optimising the most efficient elements of previous forward scatter μPIV systems. Namely, we minimised light losses along the optical train of the illumination system through the use of the condenser stage of a minimally modified transmitted light microscope, thus reducing the power of the light source necessary to provide a given incident illumination intensity on the test section. This allowed a relatively cheaper and safer continuous LED light source to be used for the same flow application and particle observation mode. Then, by implementing an in-line back-lit forward scatter 'particle shadow' observation mode at the test section, the particle image contrast for a given incident illumination intensity was maximised. As well as increasing the SNR of the particle shadow images, this contrast optimisation allows several practical options, including (1) the use of a lower power light source for the same camera thus reducing undesirable test section heating effects or (2) the use of a less sensitive camera for the same light source. Furthermore, since diffraction artifacts and specular reflections from surfaces were eliminated by using an incoherent LED light source, and optical distortions of the ROI and total internal reflections were reduced with the refractive index matching strategy, the location of the test section walls and thus the local velocity fields could be accurately obtained from the recorded images. It should be noted that the optimal choice of tracer particle diameter depends sensitively on the system magnification and camera imagining array pixel size, and thus must be determined for each application.

Finally, μPSV provides a relatively simpler, cheaper and safer way for researchers from multi-disciplinary

backgrounds to assess the instantaneous flow fields occurring in their microfluidic devices when optical access through transparent test sections is not an issue. However, it should be noted that for cases where optical access is only available from one side, front-lit epifluorescent μPIV, back scatter μPIV, or the mixed front-lit forward scatter technique developed by Hagsäter et al. (2008) may be the only available particle imaging solutions. In particular, μPSV is well suited for biomedical lab-on-a-chip applications for a number of reasons. Firstly, the optical elements necessary for μPSV, namely a condenser and an LED light source, are now standard components of commercial transmitted light microscopes. Secondly, the contamination of biological samples with fluorescent tracer particles is no longer necessary, since light scattered by structures already suspended in the fluid, such as blood cells, can be recorded and tracked (Bitsch et al. 2005). Furthermore, due to its efficient use of the incident light and the ability to regulate the test section temperature using the refractive index correcting water pool, μPSV reduces damage to sensitive samples as a result of photo bleaching and heating.

References

Ando K, Kawaguchi H (2005) High-performance fluorescent particles prepared via miniemulsion polymerisation. J Colloid Interface Sci 285:619–626

Bitsch L, Olesen LH, Westergaard CH, Bruus H, Klank H, Kutter JP (2005) Micro particle-image velocimetry of bead suspensions and blood flows. Exp Fluids 39:505–511

Bohren CF, Huffman DR (1983) Absorption and scattering of light by small particles. Wiley, New York

Bröder D, Sommerfeld M (2007) Planar shadow image velocimetry for the analysis of the hydrodynamics in bubbly flows. Meas Sci Technol 18:2513–1528

Budwig R (1994) Refractive index matching methods for liquid flow investigations. Exp Fluids 17:350–355

Chételat O, Kim KC (2002) Miniature particle image velocimetry system with LED in-line illumination. Meas Sci Technol 13:1006–1013

Cholemari MR (2007) Modeling and correction of peak-locking in digital PIV. Exp Fluids 42:913–922

Cierpka C, Kähler CJ (2012) Particle imaging techniques for volumetric three-component (3D3C) velocity measurements in microfluidics. J Vis 15:1–31

Estevadeordal J, Goss L (2005) PIV with LED: particle shadow velocimetry (PSV). 43rd AIAA aerospace sciences meeting and exhibit, meeting papers, 12355–12364

Estevadeordal J, Goss LP (2006) Particle shadow velocimetry. Patent application US2006/0175561A1

Hagsäter SM, Westergaard CH, Bruus H, Kutter JP (2008) Investigations on LED illumination for micro-PIV including a novel front lit configuration. Exp Fluids 44:211–219

Inoué S, Spring KR (1997) Video microscopy, 2nd ed. Plenum Press, Oxford

JPIV (2012) Java Particle Image Velocimetry. http://www.jpiv.vennemann-online.de

Kloosterman A, Poelma C, Westerweel J (2011) Flow rate estimation in large depth-of-field micro-PIV. Exp Fluids 50:1587–1599

Koutsiaris AG, Mathioulakis DS, Tsangaris S (1999) Microscope PIV for velocity-field measurement of particle suspensions flowing inside glass capillaries. Meas Sci Technol 10:1037–1046

Lindken R, Merzkirch W (2002) A novel PIV technique for measurements in multiphase flows and its application to two-phase bubbly flows. Exp Fluids 33:814–825

Lindken R, Rossi M, Grosse S, Westerweel J (2009) Micro-particle image velocimetry (μPIV): recent developments, applications, and guidelines. Lab Chip 9:2551–2567

Meinhart CD, Wereley ST, Gray MHB (2000) Volume illumination for two-dimensional particle image velocimetry. Meas Sci Technol 11:809–814

Meinhart CD, Wereley ST, Santiago JG (2000) A PIV algorithm for estimating time-averaged velocity fields. J Fluids Eng 122:285–289

Nikon (2012) Introduction to fluorescence microscopy. http://www.microscopyu.com

Nogueira S, Sousa R, Pinto A, Riethmuller M, Campos J (2003) Simultaneous PIV and pulsed shadow technique in slug flow: a solution for optical problems. Exp Fluids 35:598–609

Olsen MG, Adrian RJ (2000) Out-of-focus effects on particle image visibility and correlation in microscopic particle image velocimetry. Exp Fluids 29:S166–S174

Ovryn B (2000) Three-dimensional forward scattering particle image velocimetry applied to microscopic field-of-view. Exp Fluids 29:S175–S184

Ovryn B, Izen SH (2000) Imaging of transparent spheres through a planar interface using a high-numerical-aperture optical microscope. J Opt Soc Am A 17:1202–1213

Raffel M, Willert CE, Wereley ST, Kompenhans J (2007) Particle image velocimetry: a practical guide. Springer, New York

Santiago JG, Wereley ST, Meinhart CD, Beebe DJ, Adrian RJ (1998) A micro particle image velocimetry system. Exp Fluids 25:316–319

Wereley ST, Meinhart CD (2010) Recent advances in micro-particle image velocimetry. Annu Rev Fluid Mech 42:557–576

Willert CE, Gharib M (1991) Digital particle image velocimetry. Exp Fluids 10:181–193

Willert C, Stasicki B, Klinner J, Moessner S (2010) Pulsed operation of high-power light emitting diodes for imaging flow velocimetry. Meas Sci Technol 21:075402

Williams SJ, Park C, Wereley ST (2010) Advances and applications on microfluidic velocimetry techniques. Microfluid Nanofluid 8:709–726